12-29-2014

Sulfur Vacancies in Photorefractive $Sn_2P_2S_6$ Crystals

Eric M. Golden
Air Force Institute of Technology

Sergey A. Basun
Air Force Research Laboratory

A. A. Grabar
Uzhgorod National University - Ukraine

I. M. Stoika
Uzhgorod National University - Ukraine

Nancy C. Giles
Air Force Institute of Technology

See next page for additional authors

Recommended Citation

Golden, E. M., Basun, S. A., Grabar, A. A., Stoika, I. M., Giles, N. C., Evans, D. R., & Halliburton, L. E. (2014). Sulfur vacancies in photorefractive Sn2P2S6 crystals. Journal of Applied Physics, 116(24), 244107. https://doi.org/10.1063/1.4904927

Sulfur vacancies in photorefractive $Sn_2P_2S_6$ crystals

Cite as: J. Appl. Phys. **116**, 244107 (2014); https://doi.org/10.1063/1.4904927
Submitted: 23 September 2014 . Accepted: 10 December 2014 . Published Online: 29 December 2014

E. M. Golden, S. A. Basun, A. A. Grabar, I. M. Stoika, N. C. Giles, D. R. Evans, and L. E. Halliburton

Sulfur vacancies in photorefractive $Sn_2P_2S_6$ crystals

E. M. Golden,[1] S. A. Basun,[2,3] A. A. Grabar,[4] I. M. Stoika,[4] N. C. Giles,[1] D. R. Evans,[2] and L. E. Halliburton[3,5,a)]

[1]*Department of Engineering Physics, Air Force Institute of Technology, Wright-Patterson Air Force Base, Ohio 45433, USA*
[2]*Air Force Research Laboratory, Materials and Manufacturing Directorate, Wright-Patterson Air Force Base, Ohio 45433, USA*
[3]*Azimuth Corporation, 4134 Linden Avenue, Suite 300, Dayton, Ohio 45431, USA*
[4]*Institute of Solid State Physics and Chemistry, Uzhgorod National University, 88 000 Uzhgorod, Ukraine*
[5]*Department of Physics and Astronomy, West Virginia University, Morgantown, West Virginia 26506, USA*

(Received 23 September 2014; accepted 10 December 2014; published online 29 December 2014)

A photoinduced electron paramagnetic resonance (EPR) spectrum in single crystals of $Sn_2P_2S_6$ (SPS) is assigned to an electron trapped at a sulfur vacancy. These vacancies are unintentionally present in undoped SPS crystals and are expected to play an important role in the photorefractive behavior of the material. Nonparamagnetic sulfur vacancies are formed during the initial growth of the crystal. Subsequent illumination below 100 K with 442 nm laser light easily converts these vacancies to EPR-active defects. The resulting $S = 1/2$ spectrum shows well-resolved and nearly isotropic hyperfine interactions with two P ions and two Sn ions. Partially resolved interactions with four additional neighboring Sn ions are also observed. Principal values of the g matrix are 1.9700, 1.8946, and 1.9006, with the corresponding principal axes along the a, b, and c directions in the crystal. The isotropic parts of the two primary ^{31}P hyperfine interactions are 19.5 and 32.6 MHz and the isotropic parts of the two primary Sn hyperfine interactions are 860 and 1320 MHz (the latter values are each an average for ^{117}Sn and ^{119}Sn). These hyperfine results suggest that singly ionized sulfur vacancies have a diffuse wave function in SPS crystals, and thus are shallow donors. Before illumination, sulfur vacancies are in the doubly ionized charge state because of compensation by unidentified acceptors. They then trap an electron during illumination. The EPR spectrum from the sulfur vacancy is destroyed when a crystal is heated above 120 K in the dark and reappears when the crystal is illuminated again at low temperature. © *2014 AIP Publishing LLC*. [http://dx.doi.org/10.1063/1.4904927]

I. INTRODUCTION

Single crystals of $Sn_2P_2S_6$ (SPS) are well suited for photorefractive applications in the red and near-infrared spectral regions.[1–3] Although many of the basic features of the photorefractive response of this material[4–12] have now been well established, participating electron and hole traps have not yet been isolated and characterized. The identities of the primary defects necessary for a strong photorefractive effect need to be established before $Sn_2P_2S_6$ can be widely used in optical devices. Undoped crystals can have a significant photorefractive effect, thus attention is focused on intrinsic defects (e.g., sulfur and tin vacancies). These intrinsic defects may form in undoped single crystals of $Sn_2P_2S_6$ during growth and it is reasonable to expect that they could have a considerable influence on the photorefractive behavior of the material. Computational studies of the intrinsic vacancies in $Sn_2P_2S_6$ have been recently reported,[13–15] but there is a lack of experimental results describing the electronic structure and thermal stabilities of the different charge states of these vacancies.

Electron paramagnetic resonance (EPR), with its high resolution and high sensitivity, is an appropriate technique to investigate the charge states of the vacancies in $Sn_2P_2S_6$ crystals that have unpaired spins.[16,17] Often, vacancies in as-grown semiconducting crystals do not initially have an unpaired spin and a sample must be exposed to light at low temperature to stably trap an electron or hole at the vacancy. This additional electron or hole then converts the vacancy to an observable paramagnetic charge state. Thus far, the only reports of EPR from $Sn_2P_2S_6$ crystals describe investigations of Mn^{2+} and Sb^{2+} impurities substituting for Sn^{2+} ions[18,19] and intrinsic holelike small polarons (Sn^{3+} ions) at Sn^{2+} sites.[20]

In the present paper, we describe the results of an EPR investigation of singly ionized sulfur vacancies in $Sn_2P_2S_6$ crystals. The paramagnetic charge state of the vacancy is produced at 45 K with 442 nm laser light. The regular lattice consists of isolated $(P_2S_6)^{4-}$ molecular units embedded in a background of Sn^{2+} ions. Removing a sulfur ion leaves a $(P_2S_5)^{2-}$ unit in the as-grown crystal (i.e., a doubly ionized donor) that is then able to trap an electron during the low-temperature illumination and form a $(P_2S_5)^{3-}$ unit with one unpaired spin. This unpaired electron is delocalized over the $(P_2S_5)^{3-}$ unit in a molecular orbital and also has measurable overlap onto nearby Sn^{2+} ions. The angular dependence of the EPR spectrum in three high-symmetry planes gives a complete g matrix and also shows that the primary hyperfine interactions with the two ^{31}P nuclei in the $(P_2S_5)^{3-}$ unit and

a)Author to whom correspondence should be addressed. Electronic mail: Larry.Halliburton@mail.wvu.edu.

the neighboring Sn nuclei are nearly isotropic. Information about the stability of the singly ionized sulfur vacancy is obtained from an isochronal pulsed thermal anneal study.

The EPR spectrum reported in the present paper has been previously observed in single crystals of $Sn_2P_2S_6$. Ruediger *et al.*,[21,22] in an early study, suggested that the responsible defect was a Sn^{3+} ($5s^1$) ion (i.e., a holelike small polaron). Recently, however, Brant *et al.*[20] assigned a different EPR spectrum in $Sn_2P_2S_6$ to photoinduced Sn^{3+} ions (the spectrum analyzed by Brant *et al.*[20] has a large hyperfine interaction with only one Sn nucleus and no resolved ^{31}P interactions, thus clearly establishing its identity as Sn^{3+}). As a result, a "new" model was needed for the EPR spectrum initially reported by Ruediger *et al.*[21,22] and described in detail in the present paper. Our observations of large electronlike g shifts and well-resolved hyperfine interactions with two P ions and two Sn ions suggest that the correct assignment is a singly ionized sulfur vacancy.

II. EXPERIMENTAL DETAILS

Undoped single crystals of $Sn_2P_2S_6$ were grown for this study by the vertical Bridgman method at Uzhgorod National University. These included stoichiometric, sulfur-deficient, and tin-deficient boules. These crystals were grown in sealed quartz ampoules 7–8 cm in length using a small oriented seed crystal and previously sintered polycrystalline compositions as starting material. The hot and cold zones were 1100 and 920 K, respectively, and the ampoule moved at 15 mm/day. After crystallization, the boules were slowly cooled, with an anneal for several days at 500–600 K. Yellow-colored single crystals with typical lengths of 2–3 cm and diameters of 1.2–1.5 cm were produced using this method.

After orienting with the x-ray Laue technique, samples with approximate dimensions of $1.5 \times 2.0 \times 3.0\,mm^3$ were cut from larger boules for use in EPR experiments. The spectra shown in the present paper were obtained from a stoichiometric sample. Early in our investigation, we surveyed a large number of $Sn_2P_2S_6$ crystals grown by either the vapor transport method or the Bridgman method and found that the photoinduced sulfur-vacancy EPR spectrum was always present. Based on these observations, we expect that the sulfur vacancy may play an important charge-trapping role in the photorefractive response of $Sn_2P_2S_6$ crystals.

The EPR data were acquired with a Bruker EMX spectrometer operating near 9.395 GHz, while an Oxford helium-gas flow system controlled the temperature. A proton NMR teslameter was used to measure the static magnetic field. Corrections for small differences in field strength between the position of the sample and the tip of the teslameter probe were obtained by replacing the $Sn_2P_2S_6$ sample in the microwave cavity with a Cr-doped MgO crystal (the Cr^{3+} ions have a known isotropic g value of 1.9800). The $Sn_2P_2S_6$ samples were illuminated at low temperature in the microwave cavity with 442 nm light from a He-Cd laser. This photon energy is above the ~2.3 eV optical band gap of $Sn_2P_2S_6$.[4,9] We expect, however, that near-band-edge luminescence produced at low temperature by the incident 442 nm light will penetrate through the crystal and create a uniform distribution of paramagnetic sulfur vacancies.

At room temperature and below, the $Sn_2P_2S_6$ crystals are monoclinic with space group Pn and point group m (room-temperature lattice constants are $a = 9.378$ Å, $b = 7.488$ Å, $c = 6.513$ Å, and $\beta = 91.15°$).[23,24] The b axis is perpendicular to the crystal's mirror plane. In our analysis of the angular dependence of the EPR spectrum, the slight deviation from 90° between the a and c axes is disregarded. Figure 1 is a schematic representation of the $Sn_2P_2S_6$ lattice. The $(P_2S_6)^{4-}$ anionic groups with strong covalent behavior are separated by the ionic Sn^{2+} ions.[25,26] There are two inequivalent tin sites, two inequivalent phosphorus sites, and six inequivalent sulfur sites in the low-temperature phase of this material. In the higher-temperature phase (above 337 K), the tin sites are all equivalent.

III. EPR RESULTS

Figure 2 shows a photoinduced EPR spectrum from the singly ionized sulfur vacancies in a $Sn_2P_2S_6$ crystal. These data were obtained at 45 K with the magnetic field aligned along the b direction in the crystal (442 nm laser light was incident on the sample while the spectrum was recorded). This EPR signal was not present before the illumination. The key to determining a model of the defect responsible for the spectrum in Fig. 2 lies in its resolved hyperfine structure. Within the $Sn_2P_2S_6$ lattice, phosphorus has one isotope with a magnetic nucleus (^{31}P with $I = 1/2$ and 100% abundant) and tin has two isotopes with magnetic nuclei (^{117}Sn with $I = 1/2$ and 7.68% abundance and ^{119}Sn with $I = 1/2$ and 8.59% abundance). A third tin isotope (^{115}Sn with $I = 1/2$ and 0.34% abundance) and the sulfur nuclei with a magnetic moment (^{33}S with $I = 3/2$ and 0.75% abundance) can be neglected in our study. There are primary hyperfine interactions with two Sn ions and two P ions in the spectrum shown in Fig. 2. Additional less-resolved lines representing small hyperfine interactions with four more-distant Sn ions are also present in this spectrum.

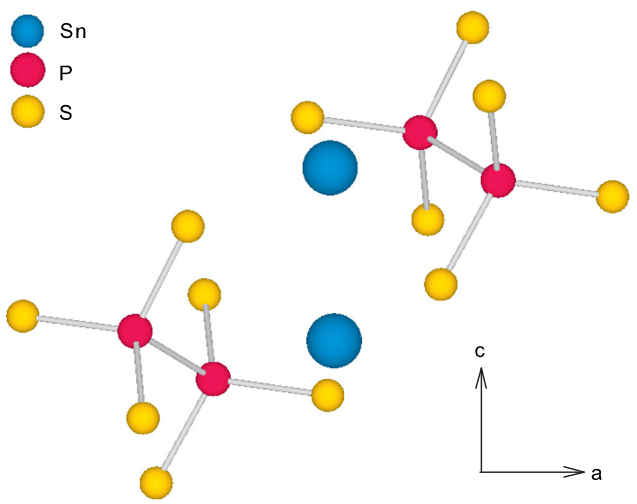

FIG. 1. A projection on the b plane of the monoclinic crystal structure of $Sn_2P_2S_6$. The crystal consists of $(P_2S_6)^{4-}$ anionic groups and Sn^{2+} cations.

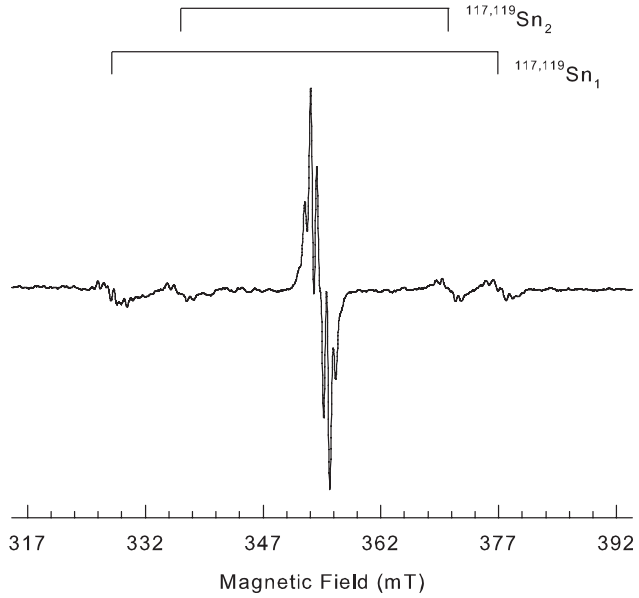

FIG. 2. EPR spectrum from singly ionized sulfur vacancies in a $Sn_2P_2S_6$ crystal. These data were taken at 45 K with the magnetic field along the *b* direction and a microwave frequency of 9.394 GHz. The sample was exposed to 442 nm laser light while acquiring the spectrum.

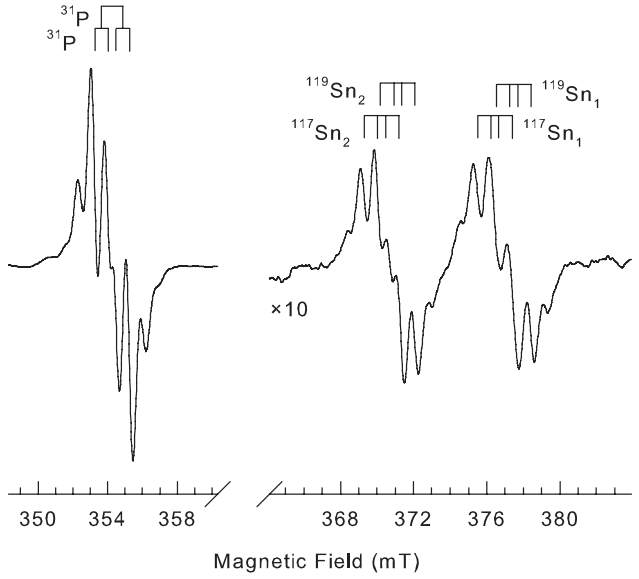

FIG. 3. Expanded view of the middle and high-field portions of the *b*-axis EPR spectrum shown in Fig. 2. The intensities of the Sn-related groups at higher magnetic field are increased by a factor of 10. Stick diagrams identify hyperfine lines from the ^{31}P, ^{117}Sn, and ^{119}Sn nuclei.

A brief examination of the *b*-axis EPR spectrum in Fig. 2 reveals a large center group of lines with two surrounding pairs of less-intense groups of lines. The outer pair of these smaller lines, located near 327 and 377 mT, are a result of the ^{117}Sn and ^{119}Sn hyperfine interactions with nuclei at a neighboring Sn site labeled Sn_1. The other widely split pair of smaller lines near 336 and 371 mT are from ^{117}Sn and ^{119}Sn hyperfine interactions with nuclei at a second neighboring Sn site labeled Sn_2. Stick diagrams above the spectrum in Fig. 2 identify these two pairs of lines. Because the sum of the natural abundances of the ^{117}Sn and ^{119}Sn nuclei is much less than 100%, an intense center group of lines from Sn nuclei with $I = 0$ (e.g., ^{116}Sn, ^{118}Sn, and ^{120}Sn) must also be present in the sulfur-vacancy spectrum. In Fig. 2, this center group is located near 354.5 mT and is due to sulfur vacancies without ^{117}Sn or ^{119}Sn nuclei at neighboring Sn_1 and Sn_2 sites. As expected for large hyperfine interactions, the widely split pairs of ^{117}Sn and ^{119}Sn lines from the Sn_1 and Sn_2 neighbors are not exactly centered on the central $I = 0$ group, but instead have their midpoint displaced slightly to lower magnetic field.

Partially resolved hyperfine lines are present in each of the groups in Fig. 2. These lines are more easily seen in the expanded *b*-axis spectrum in Fig. 3. Here, only the large center group and the two less intense high-field groups are shown. For easier comparisons, the intensities of the two high-field groups have been increased by a factor of 10. First, consider the hyperfine structure in the center group of lines near 354.2 mT. There are four equally intense lines in this group, at 353.23, 354.00, 354.49, and 355.26 mT, with the middle two almost overlapping. This is the pattern expected for slightly inequivalent hyperfine interactions with two 100% abundant $I = 1/2$ nuclei. Thus, we assign this four-line hyperfine pattern to two ^{31}P nuclei with similar, but not equal, interactions. Although the P ions in the $(P_2S_6)^{4-}$ units in the low-temperature phase of the material occupy nearly equivalent positions and their electronic bonding with neighbors is very similar, the presence of a sulfur vacancy would cause these two P ions in the resulting P_2S_5 unit to be less equivalent and have easily distinguishable hyperfine interactions with the trapped electron. For the *b* direction in Fig. 3, the hyperfine spacing for one ^{31}P interaction is 1.26 mT (33.4 MHz) and the spacing for the other ^{31}P interaction is 0.77 mT (20.4 MHz).

We now turn to the two less-intense groups of lines at higher magnetic field in Fig. 3. The hyperfine structure in these groups near 370.5 and 376.8 mT is similar, but not identical, to the hyperfine structure present in the center group at 354.2 mT. Each of these higher-field groups contain hyperfine splittings from the two ^{31}P interactions (identical to the four-line pattern seen in the center group) and also effects from ^{117}Sn and ^{119}Sn interactions. Because of the additional ^{117}Sn and ^{119}Sn interactions, there are two sets of four hyperfine lines, instead of one set of four lines, contributing to each of the high-field groups in Fig. 3. Furthermore, the separation between the two sets of four lines in the group near 370.5 mT is different from the separation of the two sets of four lines in the group near 376.8 mT. This difference in separation is illustrated with the stick diagrams above the two high-field groups in Fig. 3 and occurs because ^{119}Sn has a slightly larger nuclear magnetic moment than ^{117}Sn. The Sn hyperfine interaction increases when going from the Sn_2 to Sn_1 site and the spacing between the ^{117}Sn and ^{119}Sn lines increases slightly.

Figures 4 and 5 show photoinduced EPR spectra from the sulfur vacancy taken with the magnetic field along the *a* and *c* directions, respectively. These spectra were obtained at 45 K while illuminating with 442 nm laser light. As in Fig. 3, only the large center group and the two less intense high-field groups are included. In Fig. 4, the two ^{31}P hyperfine interactions are sufficiently similar to cause an approximate

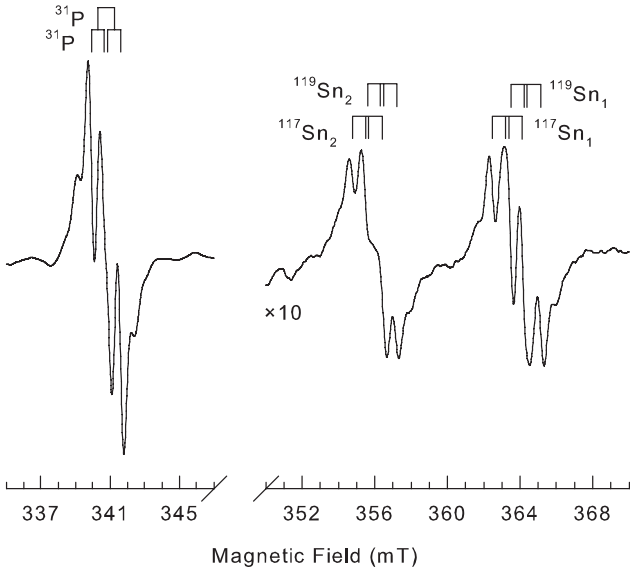

FIG. 4. Expanded view of the middle and high-field portions of the sulfur-vacancy EPR spectrum. These data were taken with the magnetic field along the *a* direction.

three-line pattern to be seen in the central group, with the central line being doubly degenerate. In contrast, the two ^{31}P hyperfine interactions in Fig. 5 are different enough to have the four lines appear well resolved in the central group. These spectra in Figs. 3–5 establish that the primary P and Sn hyperfine interactions have only a small angular dependence. The magnitudes of these interactions (deduced from the relative spacings of their hyperfine lines) are listed in Table I for spectra acquired with the magnetic field along the *a*, *b*, and *c* directions. Values for the ^{31}P interactions (these two P ions are labeled P_1 and P_2) were direct measurements of the separations of adjacent lines. Because of significant second-order shifts, values for the Sn_1 and Sn_2 interactions were obtained by matching observed separations with

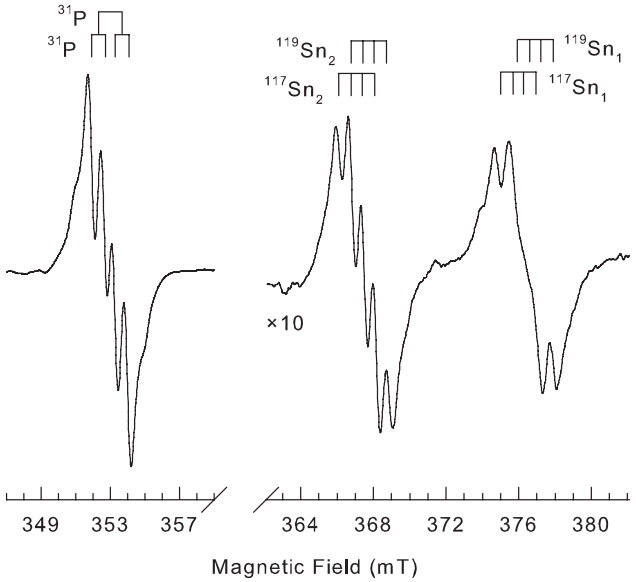

FIG. 5. Expanded view of the middle and high-field portions of the sulfur-vacancy EPR spectrum. These data were taken with the magnetic field along the *c* direction.

TABLE I. Hyperfine parameters for the primary P and Sn nuclei in the sulfur-vacancy EPR spectra in $Sn_2P_2S_6$ crystals. These results, obtained from the spectra in Figs. 3–5, represent the hyperfine separations observed when the magnetic field is along the *a*, *b*, and *c* directions. The Sn values are averages for the ^{117}Sn and ^{119}Sn interactions. Units are MHz.

	a direction	*b* direction	*c* direction
P_1	28.1	33.4	36.3
P_2	18.6	20.4	19.6
Sn_1	1358	1280	1321
Sn_2	876	910	794

solutions of a 4×4 spin Hamiltonian that included a *g* matrix and an averaged ^{117}Sn and ^{119}Sn matrix.

In the central group of lines in Fig. 3 (near 354.1 mT), additional weak hyperfine lines are present on either side of the primary set of four ^{31}P lines. These "extra" features in this *b*-axis spectrum are ^{117}Sn and ^{119}Sn hyperfine lines from the surrounding, weakly coupled, Sn ions that are more distant than Sn_1 and Sn_2. Figure 6(a) is an expanded view of the central group of lines in the actual *b*-axis spectrum and Fig. 6(b) is a simulated spectrum. The simulated spectrum was generated using the SimFonia program from Bruker and included hyperfine from two P and four distant Sn sites. In the simulation, two different ^{31}P interactions were used (20.4 and 33.4 MHz), while the four ^{117}Sn and ^{119}Sn interactions were all the same (37.1 MHz). Hyperfine interactions with the Sn_1 and Sn_2 neighbors were not included in this simulation. Stick diagrams above the spectra in Fig. 6 identify the ^{31}P lines, while the circled lines and very small lines at the highest and lowest magnetic fields are from the four distant Sn ions. Additional unresolved lines from the distant Sn are under the four ^{31}P lines. Reasonable agreement between the experimental and simulated spectra in Fig. 6 verifies that the smaller intensity lines just outside the four primary ^{31}P lines

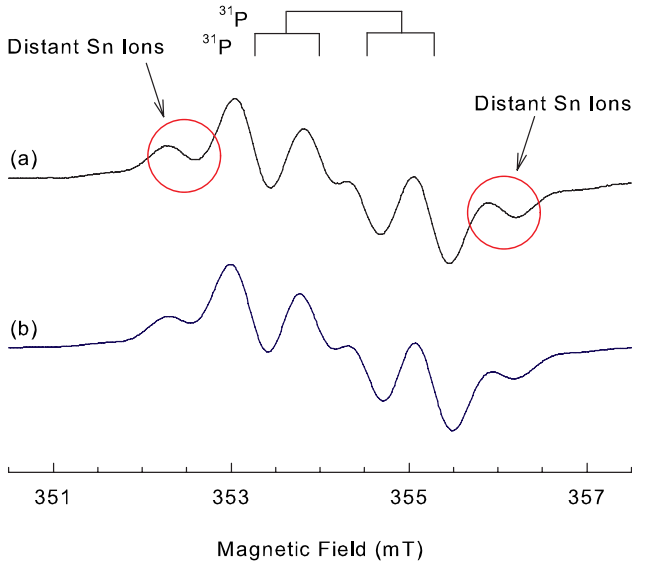

FIG. 6. Evidence for the existence of weak hyperfine interactions with more distant Sn ions. (a) Experimental EPR spectrum taken with the magnetic field along the *b* axis of the crystal. The circles identify lines from distant Sn ions. (b) Simulated EPR spectrum, including hyperfine with two phosphorus and four distant tin ions.

arise from weak interactions with more distant neighboring Sn ions. These outer weak lines are also present in the spectra taken with the field along the *a* and *c* directions (Figs. 4 and 5), but they are not as well resolved as in the *b*-axis spectrum.

The following general spin Hamiltonian describes the $S = 1/2$ EPR spectrum associated with the sulfur vacancy in $Sn_2P_2S_6$ crystals.

$$H = \beta \mathbf{S} \cdot \mathbf{g} \cdot \mathbf{B} + \sum_i (\mathbf{I}_i \cdot \mathbf{A}_i \cdot \mathbf{S} - g_{n,i}\beta_n \mathbf{I}_i \cdot \mathbf{B}). \quad (1)$$

It includes electron Zeeman, hyperfine, and nuclear Zeeman terms, with the summation being over all the ^{31}P, ^{117}Sn, and ^{119}Sn nuclei interacting with the unpaired electron.

The *g* matrix for the singly ionized sulfur vacancy was obtained by measuring the position of the midpoint of the central group of EPR lines while changing the direction of the magnetic field relative to the crystal axes. Data were taken at increments of 10° in three planes (*a*-*b*, *b*-*c*, and *c*-*a*). These experimental results are plotted as discrete points in Fig. 7. In our monoclinic lattice, a paramagnetic point defect will have two crystallographically equivalent orientations (i.e., sites). These two orientations are magnetically equivalent when the field is along the *a*, *b*, or *c* directions, and they are magnetically equivalent when the field is rotated in the *a*-*c* plane. If the principal axes of the defect's *g* matrix are along arbitrary directions, the two orientations of the defect are magnetically inequivalent when the magnetic field is rotated from *b* toward *a* or toward *c* (i.e., in the *a*-*b* and *b*-*c* planes). This would cause the defect's EPR spectrum to separate into two branches for these planes. In our present case of the sulfur vacancy, we did not observe a measurable splitting into two branches when rotating the direction of the magnetic field in the *a*-*b* and *b*-*c* planes. (Small distortions were observed in the EPR line shapes when rotating in the *b*-*c* plane, but two branches could not be resolved.) This means that the *g* matrix has a principal axis along, or very near, the *b* direction in the crystal (i.e., the direction perpendicular to the crystal's mirror plane). In Fig. 7, the angular dependence has a turning point when the magnetic field is along the *a* direction, both for rotation toward *b* and toward *c*. This requires a principal axis of the *g* matrix to be along the *a* direction in the crystal. The third principal axis must be along the *c* direction, thus forming an orthogonal set. There is an uncertainty of ±1° in the direction of the principal axis along *a*. Uncertainties in the directions of the other principal axes (along b and c) are greater, perhaps as large as ±5°, because of the possibility of slightly separated branches in the *b*-*c* plane in Fig. 7.

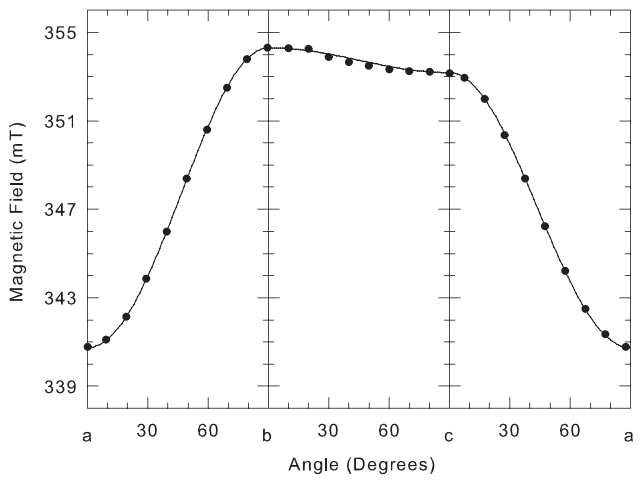

FIG. 7. Angular dependence associated with the *g* matrix of the sulfur-vacancy EPR spectrum. The midpoint of the center group of lines is plotted as a function of angle for rotations in the *a*-*b*, *b*-*c*, and *c*-*a* planes. Solid curves were calculated using the *g*-matrix parameters listed in Sec. III and a microwave frequency of 9.395 GHz. Discrete points are experimental results.

Once the directions of the principal axes of the *g* matrix were known, the principal values were obtained from measurements of the position of the central group of lines when the magnetic field was in these three directions (i.e., the *a*, *b*, and *c* directions). This gave principal values of 1.9700, 1.8946, and 1.9006, respectively, for the *a*, *b*, and *c* principal-axis directions. Estimates of uncertainties in these *g* values are ±0.0005. The solid lines in Fig. 7 were computer-generated using these principal values and axes. Good agreement between the discrete experimental points and calculated curves in Fig. 7 verifies that the correct *g* matrix has been determined. A similar detailed analysis of the hyperfine angular dependence was not attempted.

An activation energy describing the thermal decay of the singly ionized sulfur vacancy was not determined in our investigation, as it is not easily and directly measured with EPR. We did observe that the EPR spectrum from the sulfur vacancy was thermally destroyed when the crystal was held for approximately 1 min at 120 K. In this experiment, the sample was initially illuminated at 45 K. Then, the light was removed and an EPR spectrum was taken at 45 K. Next, the sample temperature was increased to 120 K, held for 1 min, and then returned to 45 K where the EPR spectrum was again taken. It is not known whether the observed decay was initiated by the release of electrons from sulfur vacancies or the release of holes from unidentified hole traps that were photocharged at the same time as the sulfur vacancies. The thermal-decay behavior of the photoinduced singly ionized sulfur vacancies may vary in other $Sn_2P_2S_6$ crystals that have different types (and different relative concentrations) of electron and hole traps.

IV. DISCUSSION

Our EPR spectra in Figs. 2–5 from $Sn_2P_2S_6$ describe an $S = 1/2$ photoinduced defect that has resolved primary hyperfine interactions with two phosphorus (P) ions and two tin (Sn) ions, along with weaker interactions with four additional tin ions. The observation of this spectrum in a variety of doped and undoped $Sn_2P_2S_6$ crystals grown by different methods implies that the defect is intrinsic, and the negative *g* shifts associated with the spectrum (i.e., the *g* values are less than 2.0023) indicate that the defect is electronlike. Together, these features suggest that the responsible defect is a singly ionized sulfur vacancy.

The alternative model of a singly ionized tin vacancy, where the unpaired spin (i.e., the hole) would be largely

localized on an adjacent sulfur ion, is much less likely for the following reasons. First, as predicted by Ruediger,[22] an EPR spectrum from the tin vacancy is expected to have positive g shifts (g values > 2.0023), whereas the defect responsible for the spectra in the present paper has large negative g shifts. Second, we found that the concentration of our defect was a factor of seven larger in a sulfur-deficient crystal, when compared to a tin-deficient crystal. To ensure a valid comparison, sample volumes and measurement conditions (e.g., temperature, modulation amplitude, microwave power, excitation light intensity, etc.) were kept the same.

Before illumination with laser light, the sulfur vacancy is in the doubly ionized charge state. The undoped $Sn_2P_2S_6$ crystals in our study are compensated and thus, in semiconductor notation, there should be singly or doubly ionized acceptors (A^- or A^{2-} acceptors) and singly or doubly ionized donors (D^+ or D^{2+} donors) before illumination. When placed in the microwave cavity at room temperature without illumination, our samples did not absorb microwaves (i.e., the Q factor of the cavity was not greatly affected). This indicates an absence of nonresonant absorption of microwaves by free carriers and verifies that the samples are heavily compensated. The presence of acceptors is consistent with earlier observations by Seres *et al.*[27] that undoped $Sn_2P_2S_6$ crystals are characterized by p-type photoconductivity. In our study, electrons move from the ionized acceptors to the ionized donors during illumination at low temperature. This converts nonparamagnetic doubly ionized sulfur vacancies (with no trapped electrons) to paramagnetic singly ionized sulfur vacancies (with one trapped electron and thus one unpaired spin).

A lack of significant angular dependence within the hyperfine patterns in the EPR spectra makes it challenging to construct a detailed model of the sulfur-vacancy defect. A $(P_2S_6)^{4-}$ unit and six neighboring Sn^{2+} ions are shown in Fig. 8 and the x, y, z fractional coordinates for these 14 ions are listed in Table II. The origin used in Table II is at the midpoint of the two phosphorus ions. Any one of the six crystallographically inequivalent sulfur sites in Fig. 8 may be vacant. Experimentally, we are unable to determine which is vacant. The general features of the sulfur-vacancy model, however, are established by considering the relative positions of the ions in Fig. 8. Table III gives the separation distances to the six nearest Sn neighbors in the regular unrelaxed lattice for each choice of position of the sulfur vacancy. For all six choices for the position of the vacancy, covalency within the $(P_2S_5)^{3-}$ unit predicts similar hyperfine interactions for the two phosphorus nuclei, in agreement with the spectra in Figs. 3–5. Our experimental ^{117}Sn and ^{119}Sn hyperfine results require that there be only two close Sn ions, thus making the Sn ions more sensitive to the sulfur-vacancy position than the P ions. According to Table III, a sulfur vacancy at the S1 or S4 positions provides a good match to experiment. Each of these vacancy positions has two close Sn ions (their separation distances range from 2.882 to 3.015 Å) and the remaining Sn ions are more than 3.801 Å away. In contrast, a sulfur vacancy at the S5 or S6 positions does not appear to be a very good match to experiment, as there are three close Sn ions with distances ranging

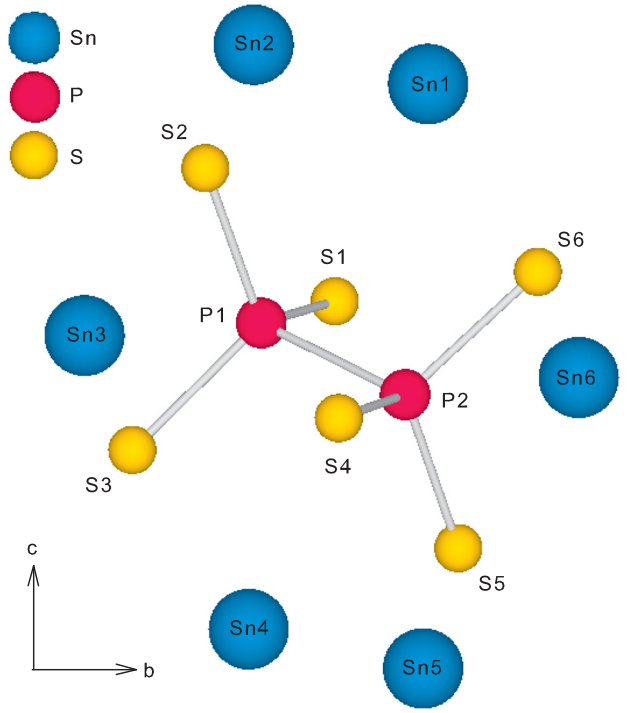

FIG. 8. Projection of the $Sn_2P_2S_6$ crystal on the a-axis, showing a $(P_2S_6)^{4-}$ unit and six nearby Sn^{2+} ions. The labeling scheme in this figure is also used in Tables II and III.

TABLE II. Fractional positions of the 14 ions shown in Fig. 8. These values are generated from the $Sn_2P_2S_6$ structural information in Ref. 23. The origin is located at the midpoint between the two P ions.

Ion	x/a	y/b	z/c
P1	−0.0669	−0.1081	0.0600
P2	0.0669	0.1081	−0.0600
S1	−0.2607	0.0017	0.0983
S2	0.0283	−0.1935	0.3242
S3	−0.0563	−0.2990	−0.1587
S4	0.2644	0.0091	−0.1011
S5	−0.0358	0.1895	−0.3220
S6	0.0545	0.3048	0.1517
Sn1	0.2765	0.1384	0.4716
Sn2	−0.2226	−0.1228	0.5362
Sn3	0.2774	−0.3718	0.0362
Sn4	−0.2226	−0.1228	−0.4638
Sn5	0.2765	0.1384	−0.5284
Sn6	−0.2235	0.3672	−0.0284

TABLE III. Distances to neighboring Sn ions for each choice of the sulfur-vacancy position. Some of the Sn ions included in this table are not among the six Sn ions shown in Fig. 8 and listed in Table II.

Sulfur vacancy	Increasing distance to six nearest Sn neighbors (in Å) →					
S1	2.882	3.015	3.801	4.836	5.120	5.165
S2	2.802	3.307	3.525	4.632	5.315	5.321
S3	2.828	3.080	3.397	4.994	5.154	5.302
S4	2.951	2.990	3.853	4.723	5.194	5.333
S5	2.943	3.053	3.269	4.959	5.071	5.512
S6	2.875	3.171	3.296	4.851	5.087	5.537

from 2.876 to 3.296 Å. In the above analysis, we have assumed that the two Sn ions responsible for the larger Sn hyperfine interactions are located close to the sulfur vacancy. However, depending on the distribution of the unpaired spin density over the $(P_2S_5)^{3-}$ molecule, it is possible that these two Sn ions could be located away from the sulfur vacancy near the opposite end of the $(P_2S_5)^{3-}$ unit.

The ^{31}P hyperfine interactions in our spectra are especially interesting. Our hyperfine parameters from Figs. 3–5 are relatively small, varying from 18.6 to 36.3 MHz for the two nuclei. They are comparable to experimental values of 41.1 MHz for the $(PS_4)^{2-}$ molecule[28] and 53.7 MHz for the $(PO_4)^{2-}$ molecule,[29] but are significantly smaller than the experimental value of 2090 MHz for a $(PO_3)^{2-}$ molecule.[30,31] In general, the magnitudes of the ^{31}P hyperfine parameters depend on the distribution of unpaired spin within the molecule. Our small values suggest that the unpaired spin is primarily distributed over the sulfur ions around the perimeter of the $(P_2S_5)^{3-}$ molecule. The spin could then interact with the central phosphorus ions by spin polarization of their σ-bonding electrons to give small isotropic couplings due to the *s* character of these latter orbitals.[32] There may also be contributions to the unpaired spin density from a non-negligible *d* character on the two phosphorus ions.[33]

The hyperfine interactions with the ^{117}Sn and ^{119}Sn nuclei at the Sn_1 and Sn_2 sites provide information about the delocalized nature of the unpaired spin's wave function. Table I gives $a = 1320$ MHz for the isotropic Fermi contact part of the averaged ^{117}Sn and ^{119}Sn interactions at the Sn_1 site (we use $a = (A_1 + A_2 + A_3)/3$ and assume that the A values all have the same sign). Morton and Preston[34] predict that a Sn 5*s* orbital (100% occupied) will have an averaged value of $a = 42\,950$ MHz for the ^{117}Sn and ^{119}Sn nuclei. These values indicate that approximately 3% of the unpaired spin associated with the sulfur vacancy is in a 5*s* orbital at the Sn_1 site. Similarly, Table I gives $a = 860$ MHz for the isotropic Fermi contact part of the averaged ^{117}Sn and ^{119}Sn interactions at the Sn_2 site. This, in turn, indicates that 2% of the unpaired spin is in a 5*s* orbital at the Sn_2 site. Together, approximately 5% of the unpaired spin is in 5*s* orbitals on these two Sn neighbors.

Although the principal values and principal axes were not determined for the hyperfine matrices at the Sn_1 and Sn_2 sites, the hyperfine splittings in Table I taken with the magnetic field along the crystal axes can be used to make an estimate of the contributions of the 5*p* orbitals on Sn_1 and Sn_2 to the total unpaired spin density. We take *b* (a parameter describing the anisotropic part of the hyperfine matrices) to be one-third of the difference between the largest and smallest hyperfine values in Table I. This gives averaged ^{117}Sn and ^{119}Sn values of $b = 26.0$ MHz for the Sn_1 site and $b = 38.7$ MHz for the Sn_2 site. Morton and Preston[34] predict that a Sn 5*p* orbital (100% occupied) will have an averaged hyperfine value of $b = 716.2$ MHz for the ^{117}Sn and ^{119}Sn nuclei (i.e., 2/5 of 1791 MHz). These values indicate that approximately 4% of the unpaired spin is in a 5*p* orbital at the Sn_1 site and 5% is in a 5*p* orbital at the Sn_2 site. This gives 9% of the unpaired spin in 5*p* orbitals on these two Sn neighbors. Including both *s* and *p* orbitals, our analysis suggests that 14% of the unpaired spin density is located on the two nearest Sn ions.

The portion of the unpaired spin density found in the 5*p* orbitals on the neighboring Sn ions provides a reasonable explanation of the observed large negative g shifts associated with the paramagnetic sulfur vacancy. Similar major g shifts have been reported for Sn^+ ions in KCl crystals.[35,36] These g shifts are due to the large spin-orbit coupling parameter ($\lambda = 2800\,cm^{-1}$) for Sn^+ combined with small energy splittings between the p_z ground state (or corresponding molecular orbital) and the p_x,p_y excited orbitals (or molecular orbitals) on the Sn ions.[36]

V. SUMMARY

A photoinduced EPR spectrum in undoped $Sn_2P_2S_6$ crystals has been assigned to singly ionized sulfur vacancies. These vacancies are intrinsic donors in this photorefractive material. The spectrum has negative (electronlike) *g* shifts and resolved primary hyperfine interactions with two P and two Sn neighbors. Weak hyperfine interactions with more distant Sn neighbors are also seen. The sulfur vacancies are doubly ionized donors in the as-grown crystals. They are converted to a paramagnetic charge state during a low-temperature illumination when electrons photoexcited from acceptors are trapped at the vacancies. After removing the light, these defects become thermally unstable when the temperature is raised above approximately 120 K, indicating a donor level within a few hundred meV of the conduction band.

Although our study has identified the EPR signal from the singly ionized sulfur vacancy in $Sn_2P_2S_6$, advanced density-functional-theory (DFT) calculations are needed to develop a more complete description of the ground state of this defect. These calculations will hopefully provide insight to the measured *g* shifts and the ^{31}P hyperfine parameters[37,38] and they may also resolve the question of the preferred site for the sulfur vacancy within the $Sn_2P_2S_6$ crystal.

ACKNOWLEDGMENTS

The authors thank Adam Brant for assistance in the initial stages of this research project. Work at Uzhgorod National University was supported by the European Office of Research and Development (Project P438a). The views expressed in this paper are those of the authors and do not necessarily reflect the official policy or position of the Air Force, the Department of Defense, or the United States Government.

[1]S. G. Odoulov, A. N. Shumelyuk, U. Hellwig, R. A. Rupp, A. A. Grabar, and I. M. Stoyka, J. Opt. Soc. Am. B **13**, 2352 (1996).
[2]S. G. Odoulov, A. N. Shumelyuk, U. Hellwig, R. A. Rupp, and A. A. Grabar, Opt. Lett. **21**, 752 (1996).
[3]S. G. Odoulov, A. N. Shumelyuk, G. A. Brost, and K. M. Magde, Appl. Phys. Lett. **69**, 3665 (1996).
[4]A. A. Grabar, I. V. Kedyk, M. I. Gurzan, I. M. Stoika, A. A. Molnar, and Yu. M. Vysochanskii, Opt. Commun. **188**, 187 (2001).
[5]A. Shumelyuk, S. Odoulov, D. Kip, and E. Krätzig, Appl. Phys. B **72**, 707 (2001).
[6]M. Jazbinsek, D. Haertle, G. Montemezzani, P. Gunter, A. A. Grabar, I. M. Stoika, and Y. M. Vysochanskii, J. Opt. Soc. Am. B **22**, 2459 (2005).

[7]B. Sturman, P. Mathey, H. R. Jauslin, S. Odoulov, and A. Shumelyuk, J. Opt. Soc. Am. B **24**, 1303 (2007).
[8]T. Bach, M. Jazbinšek, G. Montemezzani, P. Günter, A. A. Grabar, and Y. M. Vysochanskii, J. Opt. Soc. Am. B **24**, 1535 (2007).
[9]A. Shumelyuk, S. Odoulov, O. Oleynik, G. Brost, and A. Grabar, Appl. Phys. B **88**, 79 (2007).
[10]A. Shumelyuk, A. Hryhorashchuk, S. Odoulov, and D. R. Evans, Opt. Lett. **32**, 1959 (2007).
[11]A. Shumelyuk, M. Wesner, M. Imlau, and S. Odoulov, Appl. Phys. B **95**, 497 (2009).
[12]D. R. Evans, A. Shuymelyuk, G. Cook, and S. Odoulov, Opt. Lett. **36**, 454 (2011).
[13]Yu. Vysochanskii, K. Glukhov, K. Fedyo, and R. Yevych, Ferroelectrics **414**, 30 (2011).
[14]Yu. Vysochanskii, K. Glukhov, M. Maior, K. Fedyo, A. Kohutych, V. Betsa, I. Prits, and M. Gurzan, Ferroelectrics **418**, 124 (2011).
[15]Yu. Vysochanskii, A. Molnar, R. Yevych, K. Glukhov, and M. Medulych, Ferroelectrics **440**, 31 (2012).
[16]J. A. Weil and J. R. Bolton, *Electron Paramagnetic Resonance: Elementary Theory and Practical Applications*, 2nd ed. (John Wiley and Sons, New York, 2007).
[17]J.-M. Spaeth and H. Overhof, *Point Defects in Semiconductors and Insulators: Determination of Atomic and Electronic Structure from Paramagnetic Hyperfine Interactions*, Springer Series of Materials Science Vol. 51 (Springer, Berlin, 2003).
[18]I. N. Geifman, I. V. Kozlova, U. M. Vysochanski, V. Ya. Kofman, and O. A. Mikailo, Appl. Magn. Reson. **2**, 435 (1991).
[19]A. T. Brant, L. E. Halliburton, S. A. Basun, A. A. Grabar, S. G. Odoulov, A. Shumelyuk, N. C. Giles, and D. R. Evans, Phys. Rev. B **86**, 134109 (2012).
[20]A. T. Brant, L. E. Halliburton, N. C. Giles, S. A. Basun, A. A. Grabar, and D. R. Evans, J. Phys.: Condens. Matter **25**, 205501 (2013).
[21]A. Ruediger, O. Schirmer, S. Odoulov, A. Shumelyuk, and A. Grabar, Opt. Mater. **18**, 123 (2001).
[22]A. Rüdiger, "Light induced charge transfer processes and pyroelectric luminescence in Sn_2P_2S6," Ph.D. dissertation (University of Osnabrück, Osnabrück, Germany, 2001).
[23]G. Dittmar and H. Schäfer, Z. Naturforsch. **29b**, 312 (1974).
[24]B. Scott, M. Pressprich, R. D. Willet, and D. A. Cleary, J. Solid State Chem. **96**, 294 (1992).
[25]K. Kuepper, B. Schneider, V. Caciuc, M. Neumann, A. V. Postnikov, A. Ruediger, A. A. Grabar, and Yu. M. Vysochanskii, Phys. Rev. B **67**, 115101 (2003).
[26]K. Glukhov, K. Fedyo, J. Banys, and Y. Vysochanskii, Int. J. Mol. Sci. **13**, 14356 (2012).
[27]I. Seres, S. Stepanov, S. Mansurova, and A. Grabar, J. Opt. Soc. Am. B **17**, 1986 (2000).
[28]R. F. Picone, J. B. Raynor, and T. C. Ward, J. Chem. Soc., Dalton Trans. **1977**, 392.
[29]R. A. Serway and S. A. Marshall, J. Chem. Phys. **45**, 4098 (1966).
[30]M. M. Chirila, N. Y. Garces, L. E. Halliburton, S. G. Demos, T. A. Land, and H. B. Radousky, J. Appl. Phys. **94**, 6456 (2003).
[31]N. Y. Garces, K. T. Stevens, L. E. Halliburton, S. G. Demos, H. B. Radousky, and N. P. Zaitseva, J. Appl. Phys. **89**, 47 (2001).
[32]M. Symons, *Chemical and Biochemical Aspects of Electron-Spin Resonance Spectroscopy* (A Halsted Press Book, John Wiley and Sons, New York, 1978), p. 67.
[33]J. Weber, Y. Cornioley, and M. Geoffroy, Chem. Phys. Lett. **96**, 636 (1983).
[34]J. R. Morton and K. F. Preston, J. Magn. Reson. **30**, 577 (1978).
[35]C. J. Delbecq, R. Hartford, D. Schoemaker, and P. H. Yuster, Phys. Rev. B **13**, 3631 (1976).
[36]D. Schoemaker, I. Heynderickx, and E. Goovaerts, Phys. Rev. B **31**, 5687 (1985).
[37]M. T. Nguyen, S. Creve, and L. G. Vanquickenborne, J. Phys. Chem. A **101**, 3174 (1997).
[38]L. Hermosilla, P. Calle, J. M. García de la Vega, and C. Sieiro, J. Phys. Chem. A **109**, 7626 (2005).